ChemComm

COMMUNICATION

View Article Online
View Journal

Cite this: DOI: 10.1039/d5cc03052h

Received 3rd June 2025,
Accepted 12th July 2025

DOI: 10.1039/d5cc03052h

rsc.li/chemcomm

ROS-responsive SERS probes for real-time monitoring of oxidative stress in traumatic brain injury†

Dianqi Zhang,‡[ab] Li Zhou,‡[ab] Zhun Nie,‡[ab] Wei Zhang,[ab] Fabiao Yu *[ab] and Rui Wang*[ab]

We report a ROS-responsive SERS probe enabling real-time, spatiotemporal monitoring of oxidative stress in traumatic brain injury. The probe offers highly sensitive and biocompatible detection in living bEnd.3 cells and mice models, providing a powerful tool for dynamic redox analysis in biological systems.

Traumatic brain injury (TBI) is still a leading cause of death and disability worldwide, often accompanied by complex secondary injuries including neuroinflammation, oxidative stress and blood–brain barrier disruption.[1–3] Among these, the excessive production of reactive oxygen species (ROS) has been recognized as an important biological event, causing cellular damage, mitochondrial dysfunction, and long-term neurodegeneration.[4,5] Great efforts have been devoted to developing sensitive assays for detecting ROS, such as fluorescence assay,[6–8] and electrochemical assay.[9,10] Fluorescent probes such as DCFH-DA are widely used for the detection of ROS due to the deep-penetration and visual localization.[11] However, the probes often suffer from photobleaching, which may generate background noise.[12] Electrochemical sensors allow real-time quantification and highly sensitive detection.[13,14] Unfortunately, the electrochemical signals usually undergo interference from other components. Thus, conventional methods can't fully meet the requirement for detecting ROS *in vivo*, especially in the TBI models.

To overcome these limitations, surface-enhanced Raman scattering (SERS) has emerged as a promising analytical technique for biological and molecular detection due to its ultrahigh sensitivity, molecular specificity with narrow characteristic bands for multiplexed detection and resistance to photobleaching for long-term monitoring.[15,16] However, the design and preparation of responsive and stable SERS probes for real-time ROS imaging, particularly in deep tissue or injury TBI models, remains technically challenging.[17–19]

Herein, we report a rationally designed ROS-responsive SERS probe composed of gold-silver core–shell nanoparticles (Au@Ag NPs) as the substrates functionalized with 5,5′-dithiobis-(2-nitrobenzoic acid) (DTNB), which enables sensitive and time-resolved detection of ROS in both living cells and animal TBI models (Fig. 1). By optimizing the Ag shell thickness through controlling the $AgNO_3$ volume, the plasmonic enhancement and signal stability of the SERS probe can be finely tuned, which is critical for sensitive detection of ROS. DTNB plays roles as both the Raman reporter molecule and response unit for ROS. We demonstrate the capability of the SERS probe for spatiotemporal imaging of ROS in both living bEnd.3 cells and

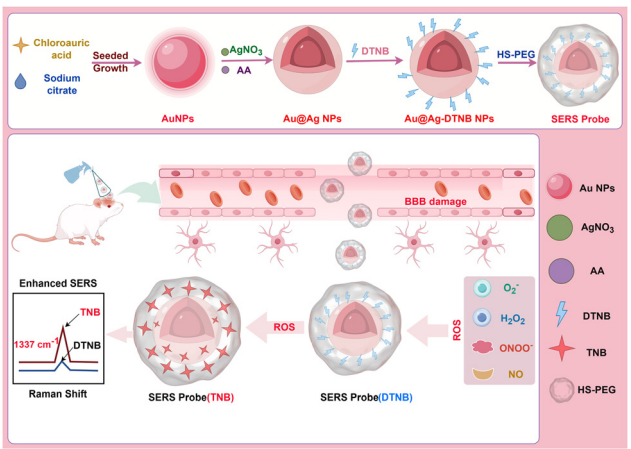

Fig. 1 Schematic illustration of the SERS probe for the detection of ROS in TBI models.

[a] *Key Laboratory of Emergency and Trauma, Ministry of Education, Key Laboratory of Hainan Trauma and Disaster Rescue, Key Laboratory of Haikou Trauma, The First Affiliated Hospital of Hainan Medical University, Hainan Medical University, Haikou 571199, China. E-mail: yufabiao@muhn.edu.cn, wangrui@muhn.edu.cn*

[b] *Engineering Research Center for Hainan Bio-Smart Materials and Bio-Medical Devices, Key Laboratory of Hainan Functional Materials and Molecular Imaging, College of Emergency and Trauma, Hainan Medical University, Haikou 571199, China*

† Electronic supplementary information (ESI) available. See DOI: https://doi.org/10.1039/d5cc03052h

‡ These authors contributed equally to this work.

in vivo mice TBI models. The probe exhibits time-dependent SERS signal enhancement corresponding to intracellular ROS accumulation without the response for antioxidant-pretreatment. Furthermore, *in vivo* SERS imaging at the injury site reveals progressive SERS signal intensities from 5 to 120 min post-probe-injection, which indicates dynamic ROS elevation associated with brain trauma. These findings have been validated by *in vitro* SERS imaging and Raman spectroscopic analysis of serum samples. Therefore, our study presents a highly sensitive, responsive SERS probe for real-time and quantitative ROS tracking in living cells and mice models, offering a useful tool for studying oxidative stress in brain trauma.

The performances of SERS active substrates play key roles for the sensitive detection.[20] To improve the detection sensitivity, the substrates used gold nanoparticles (Au NPs) and gold–silver core–shell nanoparticles (Au@Ag NPs) with various silver shell thicknesses. Fig. 2a presents digital photographs of the Au NPs and Au@Ag NPs, demonstrating distinct colour transition from wine red to yellowish-brown due to localized surface plasmon resonance (LSPR) modulation. UV-vis absorption spectra reveal a gradual blue shift in the LSPR peak from 528 nm to 450 nm, consistent with silver shell growth (Fig. 2b).[21]

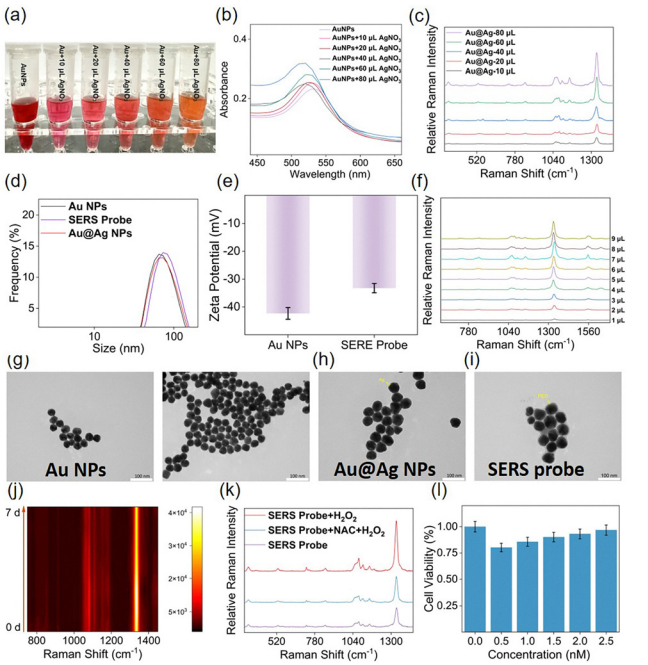

Fig. 2 (a) Digital photographs of Au NPs and core–shell structured Au@Ag NPs with different silver shell thicknesses. (b) UV-vis absorption spectra of Au@Ag NPs with different silver shell thicknesses. (c) Raman spectral characteristics of Au@Ag NPs with different silver shell thicknesses. (d) DLS particle size distribution. (e) Zeta potential test. (f) Effect of different DTNB labelling amounts on SERS signal intensity. (g) TEM images of Au NPs. (h) and (i) TEM morphology characterization of Au@Ag NPs and the SERS probe, respectively. (j) Stability test of the SERS probes for signal intensity within 7 days. (k) Comparison of Raman spectra obtained under different reaction conditions. (l) Cell viability of the SERS probe against bEnd.3 cells.

To compare the effect of Ag shell thickness on the SERS signal, the signal intensity of DTNB with various volumes of $AgNO_3$ was measured. As shown in Fig. 2c, the addition of 60 μL $AgNO_3$ shows much stronger SERS signal intensity at 1337 cm^{-1} than other volumes under the same detection conditions. Dynamic light scattering (DLS) analysis confirms the slight increase in hydrodynamic size from 60 nm to 70 nm (Fig. 2d), while zeta potential measurements exhibit a shift from −43 mV to −31 mV, indicating the successful coating on the surface of Au@Ag NPs (Fig. 2e). To optimize the labelled amount of Raman reporter molecule DTNB, various volumes (1–9 μL, 1 mM) were introduced onto the surface of the Au@Ag NPs. As indicated in Fig. 2f, variations in DTNB labelling amounts highlight optimal signal enhancement at 7 μL.

In addition, TEM images further confirm the core–shell morphology of Au@Ag NPs with a uniform Ag shell encapsulating the Au core. The stability of SERS probes usually affects the detection of the targets in the complex biological matrix.[22] The stability tests indicate stable SERS signals over 7 days in fetal bovine serum, which demonstrates the great potential of good stability in the biological milieu. The response performance of the SERS probes has been evaluated by monitoring Raman signal intensity under different conditions. As illustrated in Fig. 2k, the probe exhibits specific ROS responsiveness. H_2O_2 triggers molecular structural changes in DTNB, resulting in a significant enhancement of its characteristic peak SERS signal (Fig. S1, ESI†). The NAC control group effectively suppresses this enhancement, confirming the ROS specificity of the response. To check the biological safety of the SERS probe, cytotoxicity and *in vitro* haemolytic assessment have been performed. Cell counting kit-8 is utilized to measure the cell viability after incubation of the probe and bEnd.3 cells for 24 h. The cells still remain more than 80% (Fig. 2l). Minor fluctuations observed are within the experimental error margins and don't reflect a true increase in viability. Furthermore, the haemolytic assays demonstrate $<5\%$ haemolysis rate even at 2.5 nM (Fig. S2, ESI†). These results demonstrate good biocompatibility and potential to be used in living cells.

We investigate the influence of Ag shell thickness on the performance of the SERS probe for the detection of ROS. Ag shell thickness has been modulated by varying the volume of $AgNO_3$ during the probe synthesis. A comprehensive heatmap illustrates the Raman signal intensities obtained from the probe after reaction with different ROS concentrations (1–1000 μM) under each $AgNO_3$ volume condition (Fig. 3a). The heatmap clearly demonstrates that both the ROS concentration and Ag shell thickness play critical roles in SERS signal output. To further quantify the performance of the SERS probes under each condition, the regression coefficients (R^2) and limits of detection have been calculated as shown in Fig. 3b. The probe with 40 μL of $AgNO_3$ exhibits the most favourable performance, which can achieve an R^2 of 0.991 and the lowest LOD of 1.08 μM, indicating the optimal detection performance for further experiments. In addition, the Raman spectra after reaction with ROS consistently show the enhanced Raman intensity with increasing ROS concentration, even for the

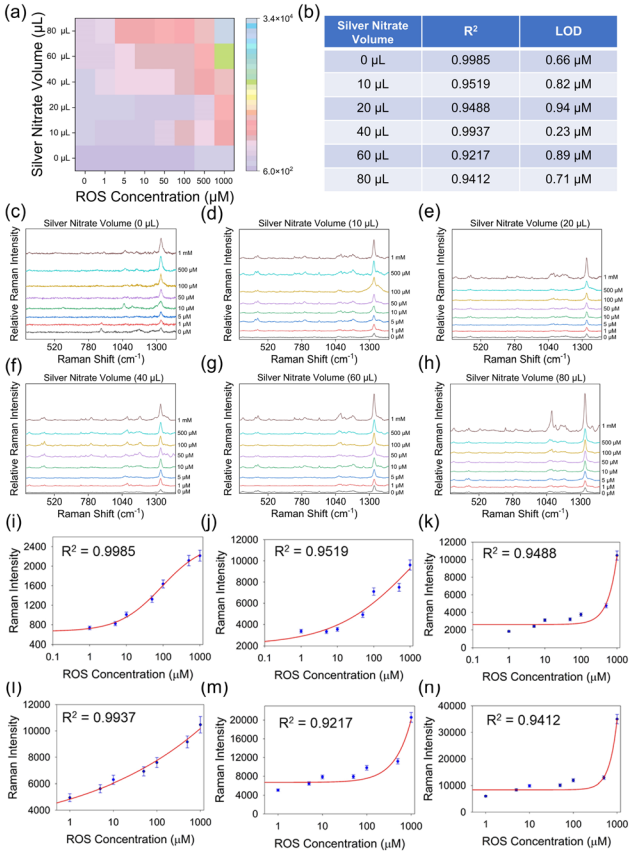

Silver Nitrate Volume	R^2	LOD
0 μL	0.9985	0.66 μM
10 μL	0.9519	0.82 μM
20 μL	0.9488	0.94 μM
40 μL	0.9937	0.23 μM
60 μL	0.9217	0.89 μM
80 μL	0.9412	0.71 μM

Fig. 3 (a) Heat map analysis of Raman signal intensity after reaction of the SERS probe with ROS for different silver shell thicknesses. (b) Evaluation of the linear regression coefficient (R^2) and limit of detection (LOD) of the SERS probe after reaction with ROS. (c)–(h) The Raman spectra of the SERS probe with different silver shell thicknesses after reaction with ROS. (i)–(n) Raman signal intensity calibration curves corresponding to (c)–(h) for quantitative analysis of the SERS probe response to ROS, respectively.

probes with different Ag shell thickness (Fig. 3c–h). To directly compare the quantitative response characteristics, the calibration curves for each Ag shell condition are presented (Fig. 3i–n). The calibration curve corresponding to 40 μL $AgNO_3$ solution not only demonstrates linearity over a wide concentration range but also maintains low standard deviation across replicate measurements, which validates the robustness of this method (Fig. 3f). In contrast, the probes with no Ag shell (0 μL, Fig. 3i) or excessive Ag shell (80 μL, Fig. 3n) exhibit decreasing performance due to the insufficient enhancement or signal saturation and background noise, respectively. Therefore, the optimal condition – 40 μL of $AgNO_3$ provides good balance between detection sensitivity and quantitative accuracy, which has great potential to be used for tracking the ROS level changes in living cells and animals.

To evaluate the response of the SERS probe toward intracellular ROS, the time-resolved SERS imaging has been conducted using bEnd.3 cells incubated with different conditions. As illustrated in Fig. S1a (ESI†), the SERS mapping images represent the dynamic intracellular distribution and SERS signal intensity of the probe alone within 120 min (Fig. S3a–c, ESI†). At the early stage (5–15 min), the SERS signals are relatively weak and sparsely distributed, suggesting the limited uptake or initial probe activation. Then, the significant increase of SERS signal intensity can be detected from 30–60 min, which indicated successful cellular internalization and activation of the probe in response to endogenous ROS. Furthermore, this trend continued to 120 min with enhanced spatial signal heterogeneity and stronger intensity. And the quantitative analysis of the Raman intensities confirms the time-dependent increase, which demonstrates that the probe exhibits the capability to detect intracellular ROS (Fig. S3d, ESI†).[23] In contrast, the bEnd.3 cells are pre-treated with *N*-acetylcysteine (NAC), a well-known antioxidant, followed by SERS probe incubation. The NAC condition serves as a negative control to evaluate whether ROS scavenging affects SERS signal changes. While a modest increase of SERS signal can still be observed over time, the overall signal intensity remains significantly lower, which can be confirmed by the quantitative analysis in Fig. S3e (ESI†) due to reduced intracellular ROS levels after incubation with NAC. The results confirm that the SERS signal changes are indeed correlated with intracellular ROS presence and are not an artefact of cellular uptake alone. Further evaluation has been provided by the incubation of the SERS probe and endogenous ROS with LPS stimulation for 30 min (Fig. S3c, ESI†).[24] The SERS signal intensities show a rapid increase as early as 10 min. In addition, the SERS signal is significantly stronger than that in the other groups, particularly at 60–120 min, which indicates enhanced ROS accumulation and higher probe activation (Fig. S3f, ESI†). All these results demonstrate that the SERS probe exhibits high reactive activation toward ROS in living cells and ROS-induced signal amplification can be quantified using SERS mapping.

To evaluate the level changes of ROS during the TBI physiological process using SERS probes, time-resolved SERS imaging has been performed in both living mice models and brain tissues. As shown in Fig. 4a, the *in vivo* SERS mapping presents pseudo-color-coded images of the injury region from 5 to 120 min post-injection. At the early stage (5–15 min), the weak SERS signals can be detected, indicating the relatively low ROS level or delayed probe activation. After post-injection for 90–120 min, the SERS signal intensities significantly increase, which is consistent with rising oxidative stress in the injured brain. The corresponding quantitative analysis also supports this trend, with a time-dependent elevation in SERS signal intensity (Fig. 4c). These results demonstrate that the proposed SERS probe can provide real-time, non-invasive monitoring of ROS in living animals. To further confirm these findings, the *in vitro* SERS imaging has been performed on brain tissues that collected at the corresponding time points of post-probe administration (Fig. 4b). The *in vitro* images display similar time-resolved increases in SERS signal intensity and spatial distribution, which indicate persistent ROS presence and probe activation even after tissue isolation. In addition, quantitative analysis confirms the rising SERS signal over time while lower than that *in vivo*, possibly due to the absence of ongoing biological activity and blood flow (Fig. 4d). In addition to

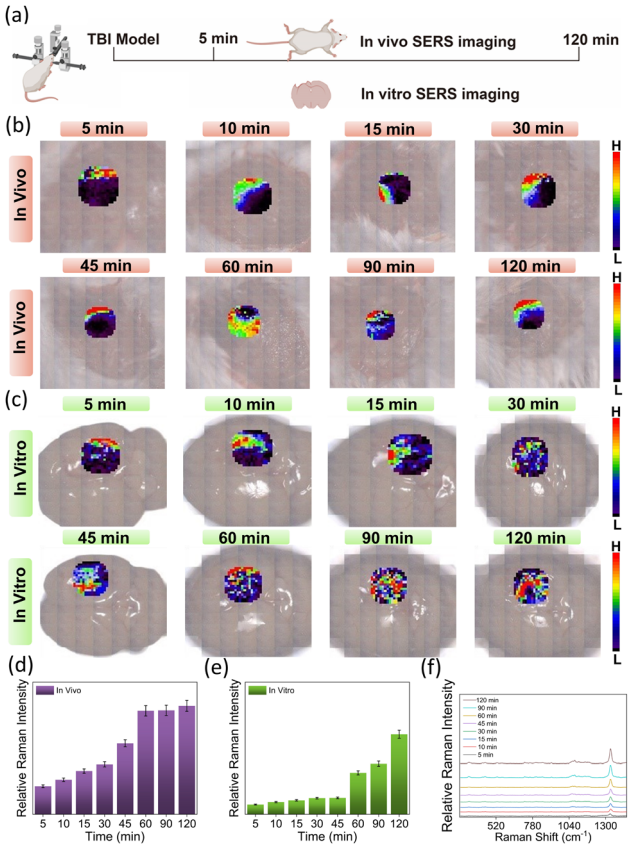

Fig. 4 (a) Schematic illustration of the SERS probe for evaluation of the ROS level changes on the TBI models. The illustration was created with the help of BioRender.com. (b) *In vivo* SERS mapping images of the corresponding pseudo-colour coding at the probe-imposed injury within 5–120 min. (c) Corresponding pseudo-colour-coded SERS mapping images of isolated brain tissue at the probe-imposed injury within 5–120 min. (d) Corresponding to (a) quantitative analysis of Raman signal intensity at different time points. (e) Quantitative analysis of Raman signal intensity at different time points corresponding to (b). (f) Raman spectral features of the SERS probe in response to serum samples collected at different time points. Statistical analysis was performed using one-way analysis of variance followed by *post hoc* Tukey multiple comparisons (n = 3, mean ± S.E.M., $^{*}P < 0.05$, $^{**}P < 0.01$, $^{***}P < 0.001$, $^{****}P < 0.0001$).

imaging data, spectral analysis of serum samples collected at the same points further confirms the probe's feasibility to ROS. As illustrated in Fig. 4e, the signal intensity of the typical Raman peak at 1337 cm^{-1} steadily increases over time, reflecting successful detection of oxidative stress markers in blood, which is associated with the ROS-responsive vibrational modes of Raman reporter molecule DTNB.

In summary, we have developed a ROS-responsive SERS probe for real-time, highly sensitive detection of oxidative stress associated with TBI. The probe successfully enables spatiotemporal mapping of ROS in both living cells and *in vivo* mice TBI models, with quantitative analysis validated through tissue imaging and serum analysis. The proposed SERS probe offers a powerful tool for studying oxidative stress in complex physiological environments.

This work is financially supported by Hainan Province Science and Technology Special Fund (No. ZDYF2024SHFZ104), Hainan Provincial Natural Science Foundation of China (825MS09), National Natural Science Foundation of China (No. 22264013), and Hainan Province Clinical Medical Center (2021).

Conflicts of interest

There are no conflicts to declare.

Data availability

The data supporting this article have been included as part of the ESI.†

Notes and references

1 Z. Doganyigit, K. Erbakan, E. Akyuz, A. K. Polat, A. Arulsamy and M. F. Shaikh, *ACS Chem. Neurosci.*, 2022, **13**, 1835–1848.
2 A. M. Cook, M. Michas and B. Robbins, *CNS Drugs*, 2025, **39**, 473–484.
3 N. Donison, J. Palik, K. Volkening and M. J. Strong, *Mol. Neurodegener.*, 2025, **20**, 56.
4 S. Li, Z. Ouyang, M. Zhang, S. Guo, B. Cai and H. Liu, *ACS Appl. Nano Mater.*, 2024, **7**, 14344–14353.
5 S. Polaka, P. Katare, B. Pawar, N. Vasdev, T. Gupta, K. Rajpoot, P. Sengupta and R. K. Tekade, *ACS Omega*, 2022, **7**, 30657–30672.
6 H. Wang, X. Wang, P. Li, M. Dong, S. Q. Yao and B. Tang, *Chem. Sci.*, 2021, **12**, 11620–11646.
7 Q. Guo, T. Wang, C. Qian and X. Wang, *Small*, 2024, **20**, 2403980.
8 Y. Zhang, X. Lv, Y. Wang, X. Chen, J. Zhang and D. Su, *Smart Mol.*, 2024, **2**, e20240031.
9 T. Zhang, Y. Liu, Y. Wang, Z. Wang, J. Liu and X. Gong, *Chem. Eng. J.*, 2023, **464**, 142443.
10 S. Zhao, G. Zang, Y. Zhang, H. Liu, N. Wang, S. Cai, C. Durkan, G. Xie and G. Wang, *Biosens. Bioelectron.*, 2021, **179**, 113052.
11 Y. Hao, J. Wang, J. Wang, Z. Guo, X. Liu, S. Lv, Q. Hu, K. Huo, Q. Yao, J. Jiang, S. Zeng, H. Kang, X. Peng, J. Yoon and H. Li, *CCS Chem.*, 2025, **7**, 1682–1697.
12 N. Kwon, D. Kim, K. M. K. Swamy and J. Yoon, *Coord. Chem. Rev.*, 2021, **427**, 213581.
13 T. Zhao, Y. P. Chen, Y. L. Xie, Y. Luo, H. Tang and J. H. Jiang, *Chem. Commun.*, 2023, **59**, 14463–14466.
14 X. Zhang, A. Oleinick, H. Jiang, Q. Liao, Q. Qiu, I. Svir, Y. Liu, C. Amatore and W. Huang, *Angew. Chem.*, 2019, **58**, 7753–7756.
15 C. Li, W. Zhang, K. Zheng and J. Guo, *Biosensors*, 2025, **15**, 115.
16 S. Laing, K. Gracie and K. Faulds, *Chem. Soc. Rev.*, 2016, **45**, 1901–1918.
17 R. Boudries, H. Williams, S. Paquereau–Gaboreau, S. Bashir, M. Hojjat Jodaylami, M. Chisanga, L.-É. Trudeau and J. F. Masson, *ACS Nano*, 2024, **18**, 22620–22647.
18 S. Elsheikh, N. P. Coles, O. J. Achadu, P. S. Filippou and A. A. Khundakar, *Biosensors*, 2024, **14**, 33.
19 D. Yang, B. Youden, N. Yu, A. J. Carrier, R. Jiang, M. R. Servos, K. D. Oakes and X. Zhang, *ACS Nano*, 2025, **19**, 2013–2028.
20 R. Goel, S. Chakraborty, V. Awasthi, V. Bhardwaj and S. K. Dubey, *Sens. Actuators, A*, 2024, **376**, 115555.
21 J. Wang, Y. Shao, C. Chen, W. Wu, D. Kong and Y. Gao, *Appl. Sci.*, 2021, **11**, 3072.
22 X. X. Han, R. S. Rodriguez, C. L. Haynes, Y. Ozaki and B. Zhao, *Nat. Rev. Methods Primers.*, 2021, **1**, 87.
23 M. I. Anik, A. Pan, M. G. Jakaria, S. A. Meenach and G. D. Bothun, *ACS Appl. Nano Mater.*, 2022, **5**, 14356–14366.
24 Y. He, M. Ye, C. Xi, J. Yu, B. Chen, H. Chen and D. Li, *ACS Sens.*, 2025, **10**, 3737–3745.

